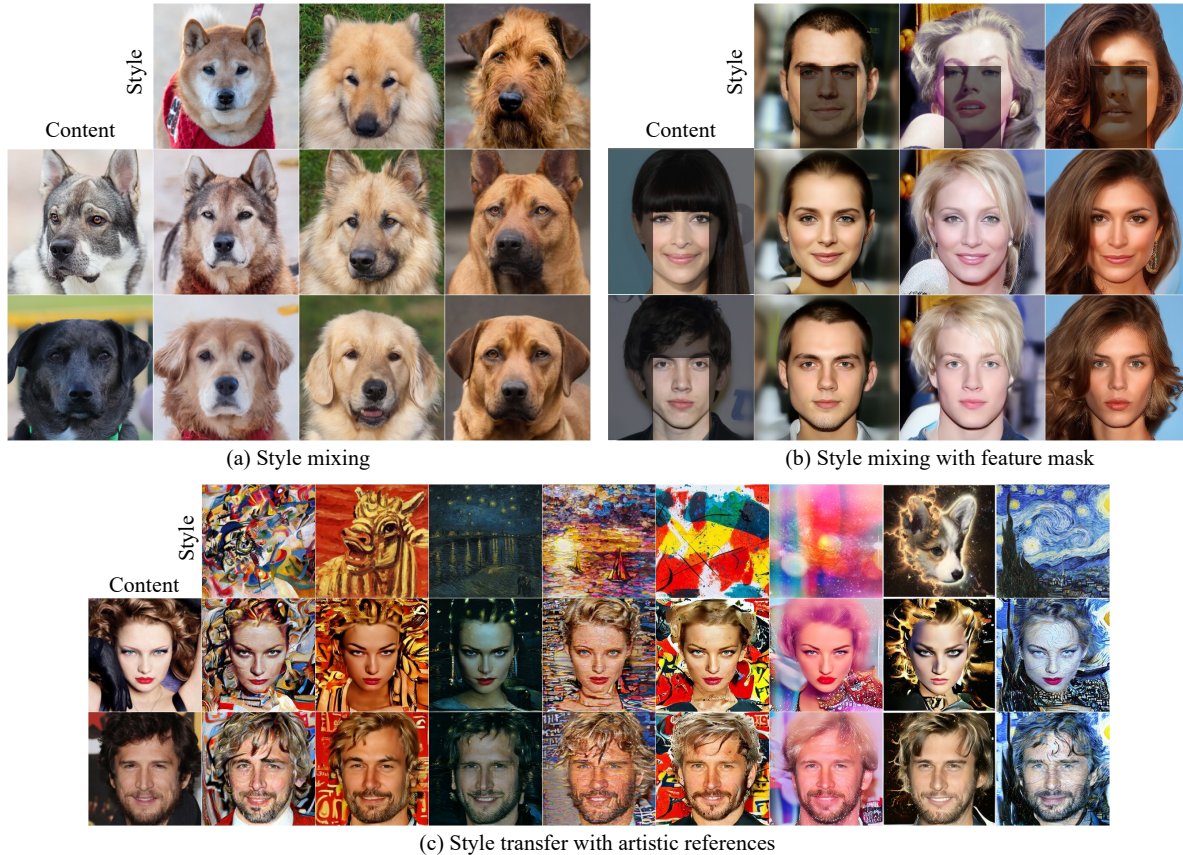


# Training-free Style Transfer Emerges from h-space in Diffusion models

Jaeseok Jeong\*

Mingi Kwon\*  
Yonsei University

Youngjung Uh



(a) Style mixing

(b) Style mixing with feature mask

(c) Style transfer with artistic references

Figure 1: DiffStyle allows (a) style mixing by content injection within the trained domain, (b) local style mixing by injecting masked content features, and (c) harmonization-like style transfer with out-of-domain style references. All results are produced by frozen pretrained diffusion models. Furthermore, flexibility of DiffStyle enables content injection into any style.

## Abstract

Diffusion models (DMs) synthesize high-quality images in various domains. However, controlling their generative process is still hazy because the intermediate variables in the process are not rigorously studied. Recently, StyleCLIP-like editing of DMs is found in the bottleneck of the U-Net, named *h-space*. In this paper, we discover that DMs inherently have disentangled representations for content and style of the resulting images: *h-space* contains the content and the skip connections convey the style. Furthermore, we introduce a principled way to inject content of one image to another considering progressive nature of the gen-

erative process. Briefly, given the original generative process, 1) the feature of the source content should be gradually blended, 2) the blended feature should be normalized to preserve the distribution, 3) the change of skip connections due to content injection should be calibrated. Then, the resulting image has the source content with the style of the original image just like image-to-image translation. Interestingly, injecting contents to styles of unseen domains produces harmonization-like style transfer. To the best of our knowledge, our method introduces the first training-free feed-forward style transfer only with an unconditional pre-trained frozen generative network. The code is available at this [our project page](#).

\*These authors contributed equally to this work

# 1. Introduction

Diffusion models (DMs) have gained recognition in various domains due to their remarkable performance in random generation [30, 69]. Naturally, researchers and practitioners seek ways to control the generative process. In this sense, text-to-image DMs provide a way to reflect a given text for generating diverse images using classifier-free guidance [57, 64, 66, 65, 5, 22]. In the same context, image guidance synthesizes random images that resemble the reference images that are given for the guidance [10, 3, 54, 55, 15]. Although these approaches provide some control, the generative process still has remaining randomness in unspecified aspects of the scene.

On the other hand, deterministic DMs, such as ODE samplers, have been used to edit real images while preserving most of the original image [69, 70, 36, 51, 53]. DiffusionCLIP [43] and Imagic [42] first embed an input image into noise and finetune DMs for editing. Still, their finetuned DMs are limited to a single attribute change or a single image, respectively. Critically, they do not provide insight into the intermediate features of DMs.

Recently, Asyrp [46] discovered a hidden latent space of pretrained DMs located at the bottleneck of the U-Net, named *h-space*. Shifting the latent feature maps along a certain direction enables semantic attribute changes, such as adding a smile. When combined with deterministic inversion, it allows real image manipulation using a pretrained frozen DM. However, its application is limited to changing certain attributes, and it does not provide as explicit operations as in generative adversarial networks, such as replacing feature maps.

In this paper, we discover that the bottleneck feature of the U-Net contains the content, and the skip connections convey the style. We design a new generative process for *content injection* given the content and style images. In Figure 1, we briefly showcase the application of content injection. Using in-domain style images produces style-mixing-like results, while using external images from the style transfer literature produces a harmonization-like effect.

Our method, named DiffStyle, blends the intermediate features of the content image in *h-space* into the generative process from the inverted style image, i.e.,  $x_T$ . It progressively combines the features with proper normalization that keeps the correlation between the skip connections and the combination along the injection. Figure 2 shows overview of our method. Additionally, we calibrate the generative process to better reflect the style elements while preserving the content.

DiffStyle enables content injection using pretrained unconditional diffusion models. Considering the bottleneck has spatial dimensions, applying DiffStyle with target region masks leads to local style mixing. To the best of our

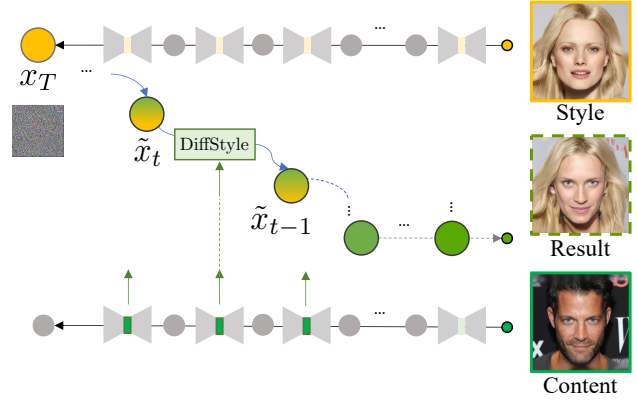


Figure 2: **Overview of DiffStyle.** During the content injection, the bottle neck feature map is recursively injected during the sampling process started from the inverted  $x_T$  of style images. The target content is reflected into the result image while preserving the original style elements.

knowledge, our method is the first to tackle these applications without additional training or extra networks. It provides convenience for users to experiment with existing pretrained DMs. In the experiments, we analyze the effect of individual components and demonstrate diverse usecases. Although there is no comparable method with perfect fit, we compare DiffStyle against closely related methods, including DiffuseIT [47].

## 2. Preliminary and related work

### 2.1. Denoising Diffusion Implicit Model (DDIM)

Diffusion models learn the distribution of data by estimating denoising score matching with  $\epsilon_t^\theta$ . In the denoising diffusion probabilistic model (DDPM) [30], the forward process is defined as a Markov process that diffuses the data through parameterized Gaussian transitions. DDIM [69] redefines DDPM as  $q_\sigma(x_{t-1}|x_t, x_0) = \mathcal{N}(\sqrt{\alpha_{t-1}}x_0 + \sqrt{1 - \alpha_{t-1} - \sigma_t^2} \cdot \frac{x_t - \sqrt{\alpha_t}x_0}{\sqrt{1 - \alpha_t}}, \sigma_t^2 \mathbf{I})$ , where  $\{\beta_t\}_{t=1}^T$  is the variance schedule and  $\alpha_t = \prod_{s=1}^t (1 - \beta_s)$ . Accordingly, the reverse process becomes:

$$x_{t-1} = \underbrace{\sqrt{\alpha_{t-1}} \left( \frac{x_t - \sqrt{1 - \alpha_t} \epsilon_t^\theta(x_t)}{\sqrt{\alpha_t}} \right)}_{\text{"predicted } x_0 \text{"}} + \underbrace{\sqrt{1 - \alpha_{t-1} - \sigma_t^2} \cdot \epsilon_t^\theta(x_t)}_{\text{"direction pointing to } x_t \text{"}} + \underbrace{\sigma_t z_t}_{\text{random noise}}, \quad (1)$$

where  $\sigma_t = \eta \sqrt{(1 - \alpha_{t-1}) / (1 - \alpha_t)} \sqrt{1 - \alpha_t / \alpha_{t-1}}$ . When  $\eta = 0$ , the process becomes deterministic.

## 2.2. Asymmetric reverse process (Asyrrp)

Asyrrp [46] introduces the asymmetric reverse process for using  $h$ -space as a semantic latent space.  $h$ -space is the bottleneck of U-Net, which is distinguished from the latent variable  $x_t$ . For real image editing, they invert  $x_0 \sim p_{real}(x)$  into  $x_T$  through the DDIM forward process, and generate  $\tilde{x}_0$  using the new  $\tilde{h}_t$  in the modified DDIM reverse process. They use an abbreviated version of Eq. (1). We follow the notation of Asyrrp throughout this paper:

$$x_{t-1} = \sqrt{\alpha_{t-1}} \mathbf{P}_t(\epsilon_t^\theta(x_t)) + \mathbf{D}_t(\epsilon_t^\theta(x_t)) + \sigma_t z_t, \quad (2)$$

where  $\mathbf{P}_t(\epsilon_t^\theta(x_t))$  denotes the predicted  $x_0$  and  $\mathbf{D}_t(\epsilon_t^\theta(x_t))$  denotes the direction pointing to  $x_t$ . We abbreviate  $\mathbf{P}_t(\epsilon_t^\theta(x_t))$  as  $\mathbf{P}_t$  and  $\mathbf{D}_t(\epsilon_t^\theta(x_t))$  as  $\mathbf{D}_t$  when the context clearly specifies the arguments. Following Asyrrp, we omit  $\sigma_t z_t$  when  $\eta = 0$ . Then, Asyrrp becomes:

$$\tilde{x}_{t-1} = \sqrt{\alpha_{t-1}} \mathbf{P}_t(\epsilon_t^\theta(\tilde{x}_t|\tilde{h}_t)) + \mathbf{D}_t(\epsilon_t^\theta(\tilde{x}_t|\tilde{h}_t)) + \sigma_t z_t, \quad (3)$$

where  $\tilde{x}_T = x_T$  and then  $\epsilon_t^\theta(\tilde{x}_t|\tilde{h}_t)$  replaces the original U-Net feature maps  $h_t$  with  $\tilde{h}_t$ . They show that the modification of  $h$ -space in both  $\mathbf{P}_t$  and  $\mathbf{D}_t$  brings a negligible change in the results. Therefore, the key idea of Asyrrp is to modify only  $h$ -space of  $\mathbf{P}_t$  while preserving  $\mathbf{D}_t$ .

Quality boosting, introduced by Asyrrp, is a stochastic noise injection when the image is almost determined. It enhances fine details and reduces the noise of images while preserving the identity of the image. The whole process of Asyrrp is as follows.

$$\tilde{x}_{t-1} = \begin{cases} \sqrt{\alpha_{t-1}} \mathbf{P}_t(\epsilon_t^\theta(\tilde{x}_t|\tilde{h}_t)) + \mathbf{D}_t & \text{if } T \geq t \geq t_{\text{edit}} \\ \sqrt{\alpha_{t-1}} \mathbf{P}_t(\epsilon_t^\theta(\tilde{x}_t|h_t)) + \mathbf{D}_t & \text{if } t_{\text{edit}} > t \geq t_{\text{boost}} \\ \sqrt{\alpha_{t-1}} \mathbf{P}_t(\epsilon_t^\theta(\tilde{x}_t|h_t)) + \mathbf{D}_t + \sigma_t^2 z & \text{if } t_{\text{boost}} > t \end{cases} \quad (4)$$

which consists of editing, denoising, and quality boosting intervals where the hyperparameter  $t_{\text{edit}}$  determines the editing interval and  $t_{\text{boost}}$  determines the quality boosting interval. Following Asyrrp, we apply quality boosting to all figures except for ablation studies.

## 2.3. Literature

After DDPMs [30] provide a universal approach for DMs, Song et al. [70] unified DMs with score-based models in SDEs. Subsequent works have focused on improving generative performance of DMs [58, 38, 11, 69, 74]. Meanwhile, ADM [20] introduced gradient-guidance to control generative process [67, 3, 52, 57], but their method does not guarantee detailed manipulation. Other works attempt to manipulate the resulting images by replacing latent variables in DMs and generating random images with the color or strokes of the desired images [10, 55] but they fall short

of content injection or style transfer. Recently, Asyrrp [46] introduced the use of the bottleneck of U-Net as a semantic latent space ( $h$ -space) through the asymmetric reverse process. However, their focus was only on semantic editing, e.g., making a person smile.

Research on image editing through the manipulation of semantic latent space has been done in other generative models such as GANs. [27, 50, 28, 8, 68, 81, 63, 24, 17] There have been a number of works that renovate GANs focusing on styles. [32, 26, 21, 9] And it is known that a semantic latent space is available for style transfers. [32, 77, 1, 33, 35, 49, 44, 41, 12, 44, 14] While most of them require fine-tuning, DiffStyle does not.

## 3. Method

In this section, we explore the interesting properties of  $h$ -space with Asyrrp [46] and design a method for content injection. We start from simply replacing  $h_t$  of one sample with that of another sample and observe its drawbacks in § 3.1. Then we introduce an important requirement for mixing two  $h_t$ 's in § 3.2. Furthermore, we propose style calibration to retain the crucial style elements in § 3.3.

### 3.1. Role of $h$ -space

$h$ -space, the deepest bottleneck of the U-Net in the diffusion models (DMs), contains the semantics of the resulting images to some extent. In other words, a change in  $h$ -space with Asyrrp [46] leads to editing the resulting image. Formally, setting  $\tilde{h}_t = h_t + \Delta h_t$  for  $t \in [T, t_{\text{edit}}]$  modifies the semantics, where  $\Delta h_t$  is the direction of desired attribute. The reverse process becomes  $\tilde{x}_{t-1} = \sqrt{\alpha_{t-1}} \mathbf{P}_t(\epsilon_t^\theta(\tilde{x}_t|\tilde{h}_t)) + \mathbf{D}_t(\epsilon_t^\theta(\tilde{x}_t|h_t))$ , where  $\tilde{h}_t = h_t + \Delta h_t^{\text{attr}}$ .

We start with a question: does  $h$  solely specify the semantics of the resulting image as in the latent codes in GANs? I.e., would replacing  $h$  totally change the output?

To answer the question, we invert two images  $I^{(1)}$  and  $I^{(2)}$  to noises  $x_T^{(1)}$  and  $x_T^{(2)}$  via forward process, respectively. Then we replace  $\{h_t\}^*$  from  $x_T^{(1)}$  with  $\{h_t^{(2)}\}$  from  $x_T^{(2)}$  during the reconstruction (i.e., reverse process). Formally,  $\tilde{x}_{t-1} = \sqrt{\alpha_{t-1}} \mathbf{P}_t(\epsilon_t^\theta(\tilde{x}_t|h_t^{(2)})) + \mathbf{D}_t(\epsilon_t^\theta(\tilde{x}_t|h_t))$ ,  $\tilde{x}_T = x_T^{(1)}$ .

Interestingly, the resulting images with the replacement contain the people in  $I^{(2)}$  with some style elements of  $I^{(1)}$  such as color distributions and backgrounds as shown in Figure 3. This phenomenon suggests that the main content is specified by  $h$  and the other aspects come from the other components, e.g., features in the skip connections. Henceforth, we name  $h_t^{(2)}$  as  $h_t^{\text{content}}$ .

\*Note that the reverse process is recursive. The reason we denote  $\{h_t\}$  instead of  $h_t^{(1)}$  is that it differs from  $h_t^{(1)}$  after the first replacement.



Figure 3: **Preliminary experiment.** Naïve replacement of  $h$  somehow combines the content and the style. However, it severely degrades image quality.

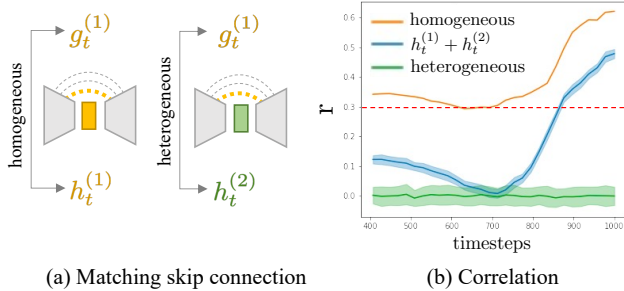


Figure 4: **Correlation between  $h_t$  and skip connection.**  $h_t$  is highly correlated with the matching skip connection. (a) illustrates examples of matching and non-matching skip connections. (b) shows correlation between each  $h_t$  and skip connection.  $r$  is Pearson correlation coefficient and p-values of  $r$  are less than  $1e-15$ . Non-matching skip connections seriously distort the correlation.

However, the replacement causes severe distortion in the images. We raise another question: how do we prevent the distortion? Note that Asyrp slightly adjusts  $h_t$  with a small change  $\Delta h_t$ . On the other hand, replacing  $h_t$  as  $h_t^{content}$  completely removes  $h_t$ . Assuming that the maintenance of  $h_t$  might be the key factor, we try an alternative in-between: adding  $h_t^{content}$  to  $h_t$ . We observe far less distortion in Figure 5 (a).

With these preliminary experiments, we hypothesize that the replacement and the addition drive the disruption of the inherent correlations in the feature map. The subsequent sections provide grounding analyses and methods to address the problem.

### 3.2. Preserving statistics with Slerp

In DMs,  $h$ -space is concatenated with skip connections and fed into the next layer. However, the previous work does not take into account the relationship between them. We observe an interesting relationship between  $h_t$  and its matching skip connections  $g_t$  within a generative process and introduce requirements for replacing  $h_t$ . We compute two versions of the correlation between the norms,  $|h_t|$  and

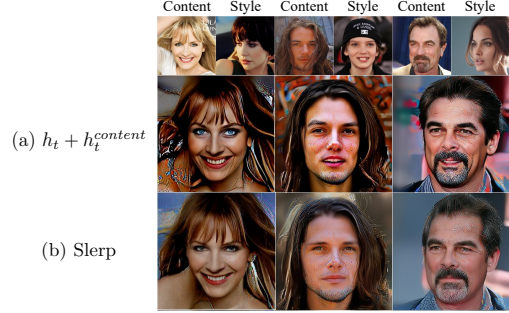


Figure 5: **Improvement in quality with Slerp.** (a) shows the result of  $h_t + h_t^{content}$ . It has some artifacts. (b) shows the result of Slerp with  $\gamma = 0.5$  brings better quality. Techniques described later are not applied here for fair comparison.

$|g_t|$ :

$$r_{\text{homo}} = \frac{\sum_i (|h^{(i)}| - |\bar{h}|) (|g^{(i)}| - |\bar{g}|)}{(n-1)s_{|h|}s_{|g|}} \quad (5)$$

$$r_{\text{hetero}} = \frac{\sum_{j \neq i} (|h^{(j)}| - |\bar{h}|) (|g^{(i)}| - |\bar{g}|)}{(n-1)s_{|h|}s_{|g|}} \quad (6)$$

where  $n$  is the number of samples and  $s_*$  denotes standard deviation of  $*$ . We omit  $t$  for brevity.

Figure 4 (b) shows that  $r_{\text{homo}}$ , the correlation between  $h_t$  and its matching skip connections, is roughly larger than 0.3 and is strongly positive when the timestep is close to  $T$ . On the other hand,  $r_{\text{hetero}}$ , the correlations between  $h_t$  and the skip connections in different samples, lie around zero. Furthermore, the alternative in-between process brings  $r_{\text{alt}}$  closer to  $r_{\text{homo}}$  by setting  $\tilde{h} = h^{(i)} + h^{(j)}$ , achieving less distortion.

Hence, we hypothesize that the correlation between  $|h|$  and  $|g|$  should remain consistent after the modification to preserve the quality of the generated images. To fulfill the hypothesis and achieve the closest difference between  $r_{\text{alt}}$  and  $r_{\text{homo}}$ , we introduce normalized spherical interpolation (Slerp) between  $h_t$  and  $h_t^{content}$ :

$$\tilde{h}_t = f(h_t, h_t^{content}, \gamma) = \text{Slerp}\left(h_t, \frac{h_t^{content}}{\|h_t^{content}\|} \cdot \|h_t\|, \gamma\right), \quad (7)$$

where  $\gamma \in [0, 1]$  is a coefficient of  $h_t^{content}$ . We note that Slerp requires the inputs to have the same norm. Normalizing  $h_t^{content}$  to match the norm of  $h_t$  ensures a consistent correlation between  $|\text{Slerp}(\cdot)|$  and  $|g_t^{(1)}|$  to be the same with the correlation between  $|h_t|$  and  $|g_t^{(1)}|$ . Replacing  $h_t$  with  $\tilde{h}_t$  using Slerp exhibits fewer artifacts and better content preservation, as shown in Figure 5 (b). Besides the improvement, we can control how much content will be injected by adjusting the  $h_t$ -to- $h_t^{content}$  ratio through parameter  $\gamma_t$  of Slerp. We provide an approximation of the total amount of injected content in § E.2.

### 3.3. Style calibration

So far, we have revealed that mixing features in  $h$ -space injects the content. Although modifying the  $h$ -space using Slerp mostly preserves the style of the original image, any changes made to the  $h$ -space inevitably affects the skip connections of the next denoising step  $t-1$ , leading to partially losing style component. Hence, we propose *style calibration* that compensates the change in the skip connections by adjusting  $\tilde{x}_t$ .

The goal of style calibration is to produce  $\tilde{x}'_{t-1}$  which better preserves the original style with the injected result. We model the implicit change from  $\tilde{x}_t$  to  $\tilde{x}'_t$  that brings similar change by the injection and introduce a hyperparameter  $\omega$  that controls the strength of the change. To this end, we define a slack variable  $\mathbf{v} = \mathbf{x}_t + d\mathbf{v}$  and find  $d\mathbf{v}$  such that  $\mathbf{P}_t(\epsilon_t^\theta(\mathbf{v})) \approx \mathbf{P}_t(\epsilon_t^\theta(\mathbf{x}_t|\tilde{\mathbf{h}}_t))$ . With the DDIM equation,

$$\sqrt{\alpha_t}\mathbf{P}_t = \mathbf{x}_t - \sqrt{1 - \alpha_t}\epsilon_t^\theta(\mathbf{x}_t), \quad (8)$$

we define infinitesimal as

$$\sqrt{\alpha_t}d\mathbf{P}_t = d\mathbf{x}_t - \sqrt{1 - \alpha_t}J(\epsilon_t^\theta)d\mathbf{x}_t. \quad (9)$$

Further letting  $d\mathbf{x}_t = \omega d\mathbf{v}$  and  $J(\epsilon_t^\theta)d\mathbf{v} = d\epsilon_t^\theta$  induces

$$d\mathbf{x}_t = \sqrt{\alpha_t}d\mathbf{P}_t + \omega\sqrt{1 - \alpha_t}d\epsilon_t^\theta. \quad (10)$$

Then, we define  $\tilde{x}'_t = \tilde{x}_t + d\mathbf{x}_t$  and obtain  $\tilde{x}'_{t-1}$  by a denoising step.

In addition,  $\mathbf{P}_t(\epsilon_t^\theta(\tilde{x}'_t))$  in Eq. (10) has larger standard deviation than  $\mathbf{P}_t(\epsilon_t^\theta(\tilde{x}_t))$ . We regularize it to have the same standard deviation of  $\mathbf{P}_t(\epsilon_t^\theta(\tilde{x}_t))$  by

$$d\mathbf{P}_t = \frac{\mathbf{P}'_t - \bar{\mathbf{P}}'_t}{|\mathbf{P}'_t|}|\mathbf{P}_t| + \bar{\mathbf{P}}'_t - \mathbf{P}_t(\epsilon_t^\theta(\tilde{x}_t)), \quad (11)$$

where  $\mathbf{P}'_t = \mathbf{P}_t(\epsilon_t^\theta(\tilde{x}'_t))$ . Then we control  $\mathbf{x}'_t$  with an  $\omega$ .

When we further expand Eq. (10),

$$d\mathbf{x}_t \approx (\omega - 1)\sqrt{1 - \alpha_t}(\epsilon_t^\theta(\tilde{x}_t|\tilde{\mathbf{h}}_t) - \epsilon_t^\theta(\tilde{x}_t)). \quad (12)$$

Interestingly, setting  $\omega = 1$  reduces  $d\mathbf{x}_t$  to  $\mathbf{0}$ , i.e., injection does not occur. And setting  $\omega \approx 0^*$  drives  $\tilde{x}'_{t-1}$  close to  $\tilde{x}_{t-1}$ , i.e., style calibration does not occur. Intuitively, by Eq. (12),  $\mathbf{x}'_t$  may share the predicted  $\mathbf{x}_0$  with  $\mathbf{P}_t(\epsilon_t^\theta(\tilde{x}_t|\tilde{\mathbf{h}}_t))$  and contains style elements. In other words, we maintain the style elements by adding  $d\mathbf{x}_t$  directly in  $x$ -space while the content injection is conducted in  $h$ -space.

Style calibration consists of four steps. First, we inject the contents as  $\tilde{x}_t \rightarrow \tilde{x}_{t-1}$ . Second, we regularize  $\mathbf{P}_t$  to preserve the original signal distribution after injection. Third, we solve the DDIM equation  $\tilde{x}'_t = \tilde{x}_t + d\mathbf{x}_t$  by using Eq. (10). Finally, we step through a reverse process  $\tilde{x}'_t \rightarrow \tilde{x}'_{t-1}$ .

\* $\omega$  can not be 0 because of its definition.

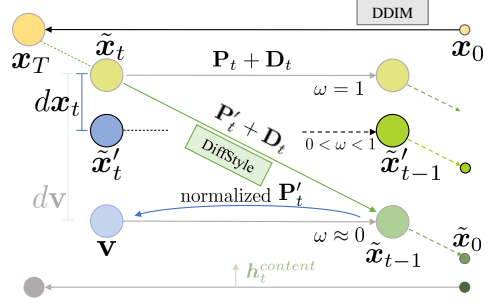


Figure 6: **Style calibration.** The result of DDIM reverse process with given approximated  $\mathbf{x}'_t$  may be similar to the result of a corresponding injected result  $\tilde{x}_{t-1}$ . As  $\omega$  gets close to 1, more style elements are added through  $d\mathbf{x}_t$ . Note that the effect of style calibration is different from modifying  $\gamma$  because it remains predicted  $\mathbf{x}_0$  by solving the DDIM equation.

### 3.4. Content injection and style transfer

We observe that  $h$ -space contains content and skip connection from  $\mathbf{x}_T$  specifies style elements. We utilize this phenomenon for content injection and style transfer. Note that it is possible to obtain inverted  $\mathbf{x}_T$  from any arbitrary real image. Therefore, even if we use out-of-domain images such as artistic images, DiffStyle successfully transfers the style of the images. Furthermore, spatial mixing of  $h$ -space enables local style mixing by injecting content into the corresponding target area. For the local style mixing, each  $\mathbf{h}_t$  is masked before Slerp and the mixed  $\mathbf{h}_t$  is inserted into the original feature map. We provide Algorithm 1 for them and an illustration of spatial  $\mathbf{h}_t$  mixing in Figure S1. Note that we omit style calibration and quality boosting [46] in the algorithm for simplicity.

---

#### Algorithm 1: DiffStyle

---

**Input:**  $\mathbf{x}_T$  (inverted latent variable from style image  $I^{style}$ ),  $\{\mathbf{h}_t^{content}\}_{t=t_{edit}}^T$  (obtained from content image  $I^{content}$ ),  $\epsilon_\theta$  (pretrained model),  $m$  (feature map mask),  $f$  (Slerp)

**Output:**  $\tilde{x}_0$  (transferred image)

- 1  $\tilde{x}_t \leftarrow \mathbf{x}_T$  **for**  $t = T, \dots, 1$  **do**
  - 2     **if**  $t \geq t_{edit}$  **then**
  - 3         Extract feature map  $\mathbf{h}_t$  from  $\epsilon_\theta(\tilde{x}_t)$ ;
  - 4          $\tilde{\mathbf{h}}_t \leftarrow f((m \otimes \mathbf{h}_t), (m \otimes \mathbf{h}_t^{content}), \gamma)$   
 $\quad \quad \quad \oplus (1 - m) \otimes \mathbf{h}_t$
  - 5          $\tilde{\epsilon} \leftarrow \epsilon_\theta(\tilde{x}_t|\tilde{\mathbf{h}}_t)$ ,  $\epsilon \leftarrow \epsilon_\theta(\tilde{x}_t)$
  - 6     **else**
  - 7          $\tilde{\epsilon} = \epsilon \leftarrow \epsilon_\theta(\tilde{x}_t)$ ,
  - 7      $\tilde{x}_{t-1} \leftarrow \sqrt{\alpha_{t-1}}(\frac{\tilde{x}_t - \sqrt{1 - \alpha_t}\tilde{\epsilon}}{\sqrt{\alpha_t}}) + \sqrt{1 - \alpha_{t-1}}\epsilon$
-

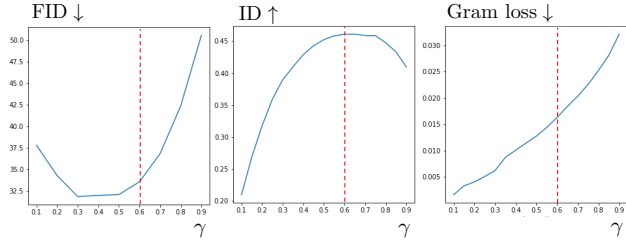


Figure 7: **Choice of  $\gamma$ .** (b) shows that  $\gamma$  should be less than 0.6 since the ID change via content injection converges at the point. If  $\gamma > 0.6$ , we only lose style faithfulness and suffer image degradation without any advantage.

## 4. Experiments

In this section, we present analyses on DiffStyle and showcase our applications.

**Setting** We use the official pretrained checkpoints of DDPM++ [70, 55] for CelebA-HQ [37] and LSUN-church/bedroom [80], iDDPM [58] for AFHQv2-Dog [13], and ADM with P2-weighting [20, 11] for METFACES [39]. The images have a resolution of  $256 \times 256$  pixels. We freeze the model weights. We use  $t_{\text{edit}}=400$ ,  $\omega=0.3$ ,  $\gamma=0.3$ , and  $t_{\text{boost}}=200$  to produce high-quality images. For more implementation details, please refer to Appendix A.

**Metrics** GRAM loss (Style loss) [26] indicates the style difference between the style image and the result image. ID computes the cosine similarity between face identity [18] of the content image and the result image to measure content consistency. Fréchet Inception Distance (FID) [29] provides the overall image quality. To compute FID, we compare generated 5K images using 50 steps of the reverse process and 25k images from a training subset of CelebA-HQ.

### 4.1. Analyses

In this section, we provide a guideline for choosing the content injection ratio considering both quality and content consistency. We also show the versatility of style calibration and propose the best interval for editing. Furthermore, we provide quantitative results which support assumptions suggested in § 3:  $h$ -space has content elements.

**Content injection ratio  $\gamma$**  We suggest that the original  $h_t$  should be partially kept in § 3.1. Figure 7 supports that the content injection ratio  $\gamma$  should be less than 0.6 for image quality (FID) and style faithfulness, and  $\gamma > 0.6$  does not increase ID similarity. We provide more observations on  $\gamma$  in Appendix B.

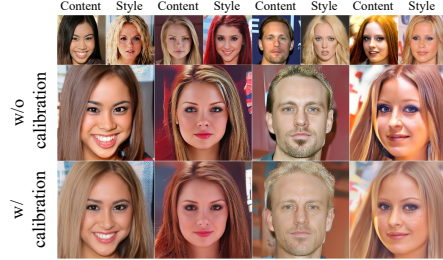


Figure 8: **Effectiveness of Style calibration.** Style calibration retains style elements while preserving content elements. We do not use other techniques such as quality boosting for comparison.

	FID ↓	ID ↑	Gram loss ↓
Reconstruction	38.71		
$h_t + h_t^{\text{content}}$	49.94	0.3581	0.0415
Lerp	36.89	0.4040	0.0318
Slerp	<b>32.09</b>	<b>0.4390</b>	<b>0.0310</b>

Table 1: **Performance of various configurations** Slerp improves FID, ID similarity between target content images and synthesized images over other methods.

**The effect of Style calibration** Figure 8 shows that style calibration leads to a better reflection of the style elements such as makeups and hair color. Note that, depending on the style calibration strength  $\omega$ , there is a trade-off relationship between Gram loss and ID similarity as well as FID. We report them at various  $\omega$  in Figure S4. We discover that increasing  $\omega$  allows more effective style transfer. More details can be found in Appendix C.

**Quantitative comparison** Table 1 shows the quantitative result of each configuration investigated in § 3. Reconstruction reports FID of the official checkpoint of DDPM++ [55] through its forward and reverse process without any modification on  $h$ -space. We observe that  $h_t + h_t^{\text{content}}$  harms FID with severe distortion. Slerp outperforms  $h_t + h_t^{\text{content}}$  in all aspects. We note that our FID score is lower than that of the reconstruction images, indicating that the quality of the generated images is similar to that of inversion images. Reconstructed images are known to have a higher FID than randomly generated images in DMs with a low number of score function evaluation (NFE). [2, 83] We suppose that the FID of our method is lower than reconstruction images because the manipulation in  $h$ -space makes the generation process closer to random generation.

Table 1 further shows the superiority of Slerp over linear interpolation (Lerp). It implies that the normalization for preserving the correlation between  $h_t$  and skips  $g_t$  is important. Furthermore, Figure S5 shows that Slerp resolves the remaining artifacts that reside in the resulting images by Lerp. Comparison between Slerp and Lerp will be further discussed in § E.1.

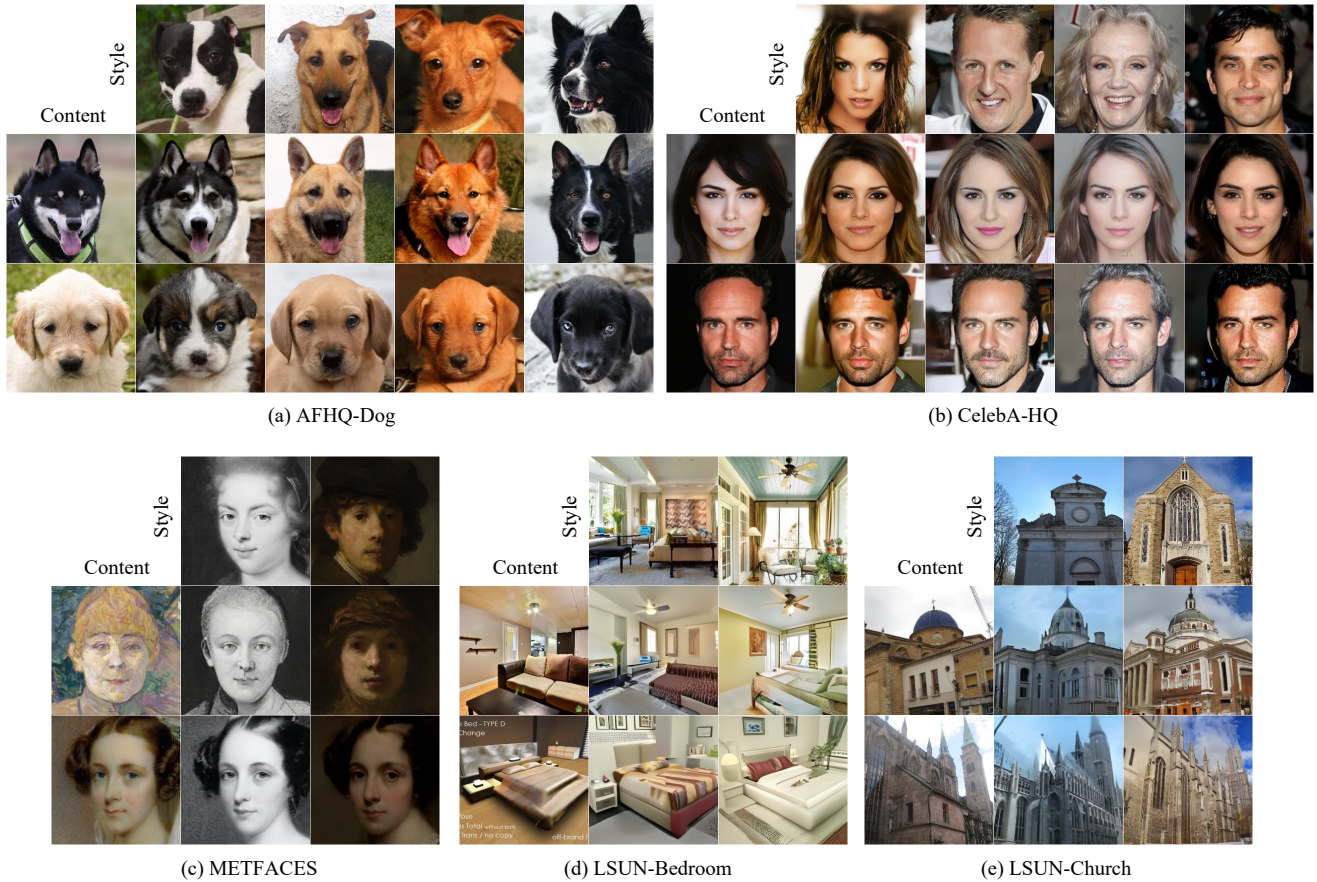


Figure 9: Qualitative results of content injection in AFHQ-Dog, CelebA-HQ LSUN-Church / Bedroom, and METFACES.

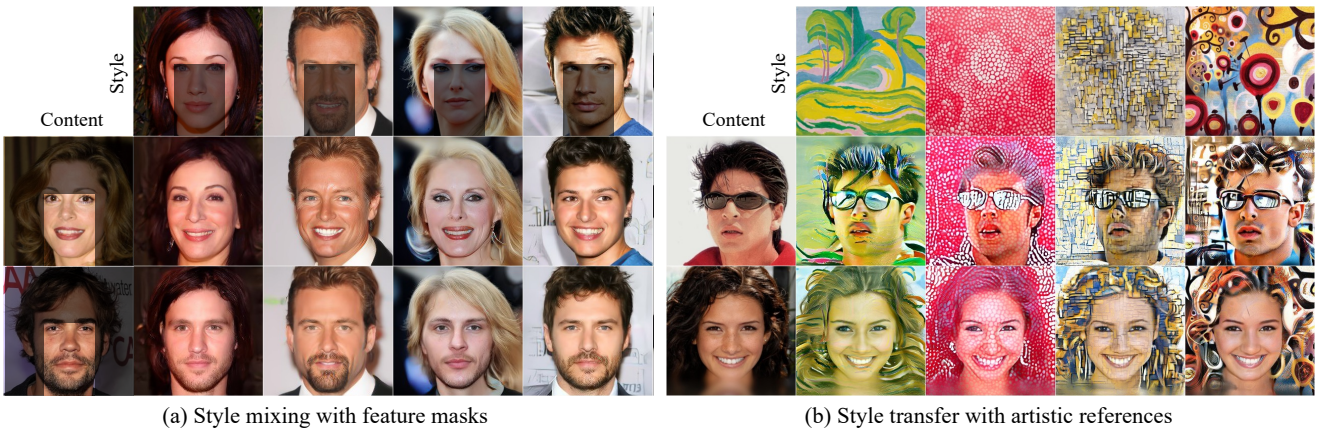


Figure 10: Qualitative results of on CelebA-HQ. We provide the results of local editing (left) and style transfer with out-of-domain images (right).

**Editing interval**  $[T, t_{\text{edit}}]$  We observe that there is a trade-off between ID similarity and Gram loss when using a suboptimal  $t_{\text{edit}}$  and specific value of  $t_{\text{edit}}$  leads to better FID, as shown in Figure 11. We choose  $t_{\text{edit}} = 400$  for its balance among the three factors. This choice also aligns

with that of Asyrp [46] for editing toward unseen domains, which requires a large change, such as injecting content. Notably, we find that  $t_{\text{edit}} = 400$  is also suitable for achieving style transfer with artistic images.

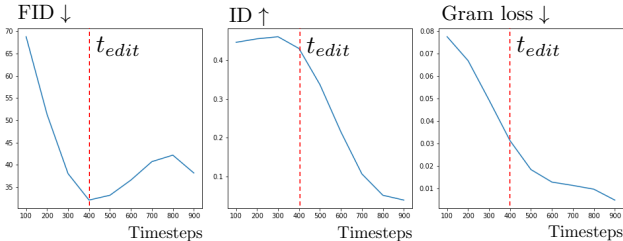


Figure 11: **Choice of  $t_{edit}$ .** We observe that  $t_{edit} = 400$  shows the best quality.



Figure 12: **Comparison with DiffuseIT** DiffStyle is effective even in situations where there is a large discrepancy between the color distributions of the style and content.

## 4.2. Applications

**Content injection** Figure 9 shows that DiffStyle works on various architectures and datasets. In Figure 10 (a), the masked content injection successfully brings the style to the desired area. See Appendix D.1 for more results.

**Style transfer** In addition, we can use arbitrary style images, even if they are out-of-domain. Figure 1 (c) and Figure 10 (b) show results with artistic images as style. In style transfer, we do not use quality boosting [46] since they aim to improve the quality and realism of  $x_0$  which may not be desirable when transferring the style of an out-of-domain image onto the target image. We provide more results in Appendix D.1.

## 4.3. Comparison with existing methods

We first note that there is no competitor with perfect compatibility: frozen pretrained diffusion models, no extra guidance from pretrained models, and versatility (content injection, masked injection, and style transfer). Still, we compare our content injection with DiffuseIT [47] which uses pretrained DINO ViT [7] for guidance. Figure 12 shows that DiffuseIT struggles when there is a large gap between the content and style regarding color distributions. More qualitative comparisons with existing methods [60, 44, 19, 75] and user study are deferred to Appendix D.2.

## 5. Conclusion and discussion

In this paper, we propose a training-free content injection and style transfer using pretrained DMs. The components

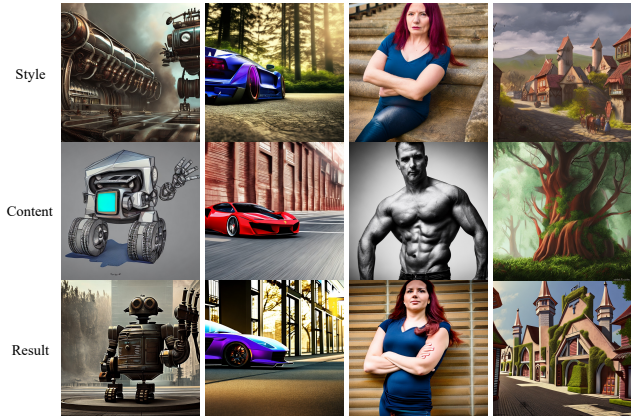


Figure 13: **DiffStyle on Stable diffusion** Although we observe similar phenomena, the content elements of latent-level DMs is different from pixel-level DMs; More semantic elements is injected to the style image.

in our method are designed to preserve the statistical properties of the original reverse process so that the resulting images are free from artifacts even when the style image is out-of-domain. We hope that our method and its analyses help the research community to harness the nice properties of DMs for various image synthesis tasks.

Although DiffStyle achieves high quality content injection, the small resolution of the  $h$ -space hinders fine control of the injecting region. We provide content injection with various masks in Figure S9.

While adopting out-of-domain images as style leads to harmonization-like style transfer, adopting content-less out-of-domain images as content leads to meaningless results. We provide them in Figure S8. We suggest that  $h_t$  is not the universal representation for arbitrary content.

In addition, we provide pilot results of DiffStyle on Stable diffusion in Figure 13. It works somewhat similarly but the phenomenon is not as clear as in non-latent diffusion models. The bottleneck of Stable diffusion appears more semantically rich, possibly due to its diffusion in VAE’s latent space. Unveiling the mechanisms in latent diffusion models remains our future work. Please refer to Appendix I for the details.

Lastly, we briefly discuss the effect of the scheduling strategy of the injecting ratio  $\gamma$  in Appendix G. Further investigation would be an interesting research direction.

## Acknowledgement

The authors thank Yong-Hyun Park for constructive discussion.



## References

- [1] Jie An, Tao Li, Haozhi Huang, Li Shen, Xuan Wang, Yongyi Tang, Jinwen Ma, Wei Liu, and Jiebo Luo. Real-time universal style transfer on high-resolution images via zero-channel pruning. *arXiv preprint arXiv:2006.09029*, 2020. **3**
- [2] Andrea Asperti, Davide Evangelista, Samuele Marro, and Fabio Merizzi. Image embedding for denoising generative models. *arXiv preprint arXiv:2301.07485*, 2022. **6**
- [3] Omri Avrahami, Dani Lischinski, and Ohad Fried. Blended diffusion for text-driven editing of natural images. In *Proceedings of the IEEE/CVF Conference on Computer Vision and Pattern Recognition*, pages 18208–18218, 2022. **2, 3, 16**
- [4] Kyungjune Baek, Yunjey Choi, Youngjung Uh, Jaejun Yoo, and Hyunjung Shim. Rethinking the truly unsupervised image-to-image translation. In *Proceedings of the IEEE/CVF International Conference on Computer Vision*, pages 14154–14163, 2021. **16**
- [5] Yogesh Balaji, Seungjun Nah, Xun Huang, Arash Vahdat, Jiaming Song, Karsten Kreis, Miika Aittala, Timo Aila, Samuli Laine, Bryan Catanzaro, et al. ediffi: Text-to-image diffusion models with an ensemble of expert denoisers. *arXiv preprint arXiv:2211.01324*, 2022. **2**
- [6] Dmitry Baranchuk, Ivan Rubachev, Andrey Voynov, Valentin Khruikov, and Artem Babenko. Label-efficient semantic segmentation with diffusion models. *arXiv preprint arXiv:2112.03126*, 2021. **16**
- [7] Mathilde Caron, Hugo Touvron, Ishan Misra, Hervé Jégou, Julien Mairal, Piotr Bojanowski, and Armand Joulin. Emerging properties in self-supervised vision transformers. In *Proceedings of the IEEE/CVF international conference on computer vision*, pages 9650–9660, 2021. **8, 14**
- [8] Hila Chefer, Sagie Benaim, Roni Paiss, and Lior Wolf. Image-based clip-guided essence transfer. *arXiv preprint arXiv:2110.12427*, 2021. **3**
- [9] Dongdong Chen, Lu Yuan, Jing Liao, Nenghai Yu, and Gang Hua. Stylebank: An explicit representation for neural image style transfer. In *Proceedings of the IEEE conference on computer vision and pattern recognition*, pages 1897–1906, 2017. **3**
- [10] Jooyoung Choi, Sungwon Kim, Yonghyun Jeong, Youngjune Gwon, and Sungroh Yoon. Ilvr: Conditioning method for denoising diffusion probabilistic models. *arXiv preprint arXiv:2108.02938*, 2021. **2, 3, 16**
- [11] Jooyoung Choi, Jungbeom Lee, Chaehun Shin, Sungwon Kim, Hyunwoo Kim, and Sungroh Yoon. Perception prioritized training of diffusion models. In *Proceedings of the IEEE/CVF Conference on Computer Vision and Pattern Recognition*, pages 11472–11481, 2022. **3, 6**
- [12] Yunjey Choi, Minje Choi, Munyoung Kim, Jung-Woo Ha, Sunghun Kim, and Jaegul Choo. Stargan: Unified generative adversarial networks for multi-domain image-to-image translation. In *Proceedings of the IEEE conference on computer vision and pattern recognition*, pages 8789–8797, 2018. **3, 16**
- [13] Yunjey Choi, Youngjung Uh, Jaejun Yoo, and Jung-Woo Ha. Stargan v2: Diverse image synthesis for multiple domains. In *Proceedings of the IEEE/CVF conference on computer vision and pattern recognition*, pages 8188–8197, 2020. **6, 16**
- [14] Min Jin Chong and David Forsyth. Jojogan: One shot face stylization. In *Computer Vision—ECCV 2022: 17th European Conference, Tel Aviv, Israel, October 23–27, 2022, Proceedings, Part XVI*, pages 128–152. Springer, 2022. **3, 16**
- [15] Hyungjin Chung, Byeongsu Sim, Dohoon Ryu, and Jong Chul Ye. Improving diffusion models for inverse problems using manifold constraints. *arXiv preprint arXiv:2206.00941*, 2022. **2**
- [16] Guillaume Couairon, Jakob Verbeek, Holger Schwenk, and Matthieu Cord. Diffedit: Diffusion-based semantic image editing with mask guidance. *arXiv preprint arXiv:2210.11427*, 2022. **16**
- [17] Ning Dai, Jianze Liang, Xipeng Qiu, and Xuanjing Huang. Style transformer: Unpaired text style transfer without disentangled latent representation. *arXiv preprint arXiv:1905.05621*, 2019. **3**
- [18] Jiankang Deng, Jia Guo, Niannan Xue, and Stefanos Zafeiriou. Arcface: Additive angular margin loss for deep face recognition. In *Proceedings of the IEEE/CVF conference on computer vision and pattern recognition*, pages 4690–4699, 2019. **6**
- [19] Yingying Deng, Fan Tang, Xingjia Pan, Weiming Dong, Chongyang Ma, and Changsheng Xu. Stytr<sup>2</sup>: Unbiased image style transfer with transformers. *arXiv preprint arXiv:2105.14576*, 2021. **8, 13**
- [20] Prafulla Dhariwal and Alexander Nichol. Diffusion models beat gans on image synthesis. *Advances in Neural Information Processing Systems*, 34:8780–8794, 2021. **3, 6**
- [21] Vincent Dumoulin, Jonathon Shlens, and Manjunath Kudlur. A learned representation for artistic style. *arXiv preprint arXiv:1610.07629*, 2016. **3**
- [22] Oran Gafni, Adam Polyak, Oron Ashual, Shelly Sheynin, Devi Parikh, and Yaniv Taigman. Make-a-scene: Scene-based text-to-image generation with human priors. *arXiv preprint arXiv:2203.13131*, 2022. **2**
- [23] Rinon Gal, Yuval Alaluf, Yuval Atzmon, Or Patashnik, Amit H Bermano, Gal Chechik, and Daniel Cohen-Or. An image is worth one word: Personalizing text-to-image generation using textual inversion. *arXiv preprint arXiv:2208.01618*, 2022. **16**
- [24] Rinon Gal, Or Patashnik, Haggai Maron, Gal Chechik, and Daniel Cohen-Or. Stylegan-nada: Clip-guided domain adaptation of image generators. *arXiv preprint arXiv:2108.00946*, 2021. **3**
- [25] Leon A Gatys, Alexander S Ecker, and Matthias Bethge. A neural algorithm of artistic style. *arXiv preprint arXiv:1508.06576*, 2015. **16**
- [26] Leon A Gatys, Alexander S Ecker, and Matthias Bethge. Image style transfer using convolutional neural networks. In *Proceedings of the IEEE conference on computer vision and pattern recognition*, pages 2414–2423, 2016. **3, 6**
- [27] Ian Goodfellow, Jean Pouget-Abadie, Mehdi Mirza, Bing Xu, David Warde-Farley, Sherjil Ozair, Aaron Courville, and Yoshua Bengio. Generative adversarial networks. *Communications of the ACM*, 63(11):139–144, 2020. **3, 16**

- [28] Erik Härkönen, Aaron Hertzmann, Jaakko Lehtinen, and Sylvain Paris. Ganspace: Discovering interpretable gan controls. *Advances in Neural Information Processing Systems*, 33:9841–9850, 2020. [3](#)
- [29] Martin Heusel, Hubert Ramsauer, Thomas Unterthiner, Bernhard Nessler, and Sepp Hochreiter. Gans trained by a two time-scale update rule converge to a local nash equilibrium. *Advances in neural information processing systems*, 30, 2017. [6](#)
- [30] Jonathan Ho, Ajay Jain, and Pieter Abbeel. Denoising diffusion probabilistic models. *Advances in Neural Information Processing Systems*, 33:6840–6851, 2020. [2](#), [3](#), [16](#)
- [31] Judy Hoffman, Eric Tzeng, Taesung Park, Jun-Yan Zhu, Phillip Isola, Kate Saenko, Alexei Efros, and Trevor Darrell. Cycada: Cycle-consistent adversarial domain adaptation. In *International conference on machine learning*, pages 1989–1998. Pmlr, 2018. [16](#)
- [32] Xun Huang and Serge Belongie. Arbitrary style transfer in real-time with adaptive instance normalization. In *Proceedings of the IEEE international conference on computer vision*, pages 1501–1510, 2017. [3](#)
- [33] Xun Huang, Ming-Yu Liu, Serge Belongie, and Jan Kautz. Multimodal unsupervised image-to-image translation. In *Proceedings of the European conference on computer vision (ECCV)*, pages 172–189, 2018. [3](#)
- [34] Phillip Isola, Jun-Yan Zhu, Tinghui Zhou, and Alexei A Efros. Image-to-image translation with conditional adversarial networks. In *Proceedings of the IEEE conference on computer vision and pattern recognition*, pages 1125–1134, 2017. [16](#)
- [35] Justin Johnson, Alexandre Alahi, and Li Fei-Fei. Perceptual losses for real-time style transfer and super-resolution. In *European conference on computer vision*, pages 694–711. Springer, 2016. [3](#)
- [36] Alexia Jolicoeur-Martineau, Ke Li, Rémi Piché-Taillefer, Tal Kachman, and Ioannis Mitliagkas. Gotta go fast when generating data with score-based models. *arXiv preprint arXiv:2105.14080*, 2021. [2](#)
- [37] Tero Karras, Timo Aila, Samuli Laine, and Jaakko Lehtinen. Progressive growing of gans for improved quality, stability, and variation. In *International Conference on Learning Representations*, 2018. [6](#), [16](#)
- [38] Tero Karras, Miika Aittala, Timo Aila, and Samuli Laine. Elucidating the design space of diffusion-based generative models. *arXiv preprint arXiv:2206.00364*, 2022. [3](#)
- [39] Tero Karras, Miika Aittala, Janne Hellsten, Samuli Laine, Jaakko Lehtinen, and Timo Aila. Training generative adversarial networks with limited data. *Advances in Neural Information Processing Systems*, 33:12104–12114, 2020. [6](#)
- [40] Tero Karras, Samuli Laine, and Timo Aila. A style-based generator architecture for generative adversarial networks. In *Proceedings of the IEEE/CVF conference on computer vision and pattern recognition*, pages 4401–4410, 2019. [16](#)
- [41] Tero Karras, Samuli Laine, Miika Aittala, Janne Hellsten, Jaakko Lehtinen, and Timo Aila. Analyzing and improving the image quality of stylegan. In *Proceedings of the IEEE/CVF conference on computer vision and pattern recognition*, pages 8110–8119, 2020. [3](#), [16](#)
- [42] Bahjat Kawar, Shiran Zada, Oran Lang, Omer Tov, Huiwen Chang, Tali Dekel, Inbar Mosseri, and Michal Irani. Imagic: Text-based real image editing with diffusion models. *arXiv preprint arXiv:2210.09276*, 2022. [2](#)
- [43] Gwanghyun Kim and Jong Chul Ye. Diffusionclip: Text-guided image manipulation using diffusion models. 2021. [2](#), [16](#)
- [44] Hyunsu Kim, Yunjei Choi, Junho Kim, Sungjoo Yoo, and Youngjung Uh. Exploiting spatial dimensions of latent in gan for real-time image editing. In *Proceedings of the IEEE/CVF Conference on Computer Vision and Pattern Recognition*, pages 852–861, 2021. [3](#), [8](#), [13](#), [16](#)
- [45] Nupur Kumari, Bingliang Zhang, Richard Zhang, Eli Shechtman, and Jun-Yan Zhu. Multi-concept customization of text-to-image diffusion. *arXiv preprint arXiv:2212.04488*, 2022. [16](#)
- [46] Gihyun Kwon and Jong Chul Ye. Diffusion-based image translation using disentangled style and content representation. *arXiv preprint arXiv:2209.15264*, 2022. [2](#), [3](#), [5](#), [7](#), [8](#), [16](#)
- [47] Gihyun Kwon and Jong Chul Ye. Diffusion-based image translation using disentangled style and content representation. *arXiv preprint arXiv:2209.15264*, 2022. [2](#), [8](#), [14](#)
- [48] Yuheng Li, Haotian Liu, Qingyang Wu, Fangzhou Mu, Jianwei Yang, Jianfeng Gao, Chunyuan Li, and Yong Jae Lee. Gligen: Open-set grounded text-to-image generation. *arXiv preprint arXiv:2301.07093*, 2023. [16](#)
- [49] Tianwei Lin, Zhuoqi Ma, Fu Li, Dongliang He, Xin Li, Errui Ding, Nannan Wang, Jie Li, and Xinbo Gao. Drafting and revision: Laplacian pyramid network for fast high-quality artistic style transfer. In *Proceedings of the IEEE/CVF Conference on Computer Vision and Pattern Recognition*, pages 5141–5150, 2021. [3](#)
- [50] Huan Ling, Karsten Kreis, Daiqing Li, Seung Wook Kim, Antonio Torralba, and Sanja Fidler. Editgan: High-precision semantic image editing. *Advances in Neural Information Processing Systems*, 34:16331–16345, 2021. [3](#)
- [51] Luping Liu, Yi Ren, Zhijie Lin, and Zhou Zhao. Pseudo numerical methods for diffusion models on manifolds. *arXiv preprint arXiv:2202.09778*, 2022. [2](#)
- [52] Xihui Liu, Dong Huk Park, Samaneh Azadi, Gong Zhang, Arman Chopikyan, Yuxiao Hu, Humphrey Shi, Anna Rohrbach, and Trevor Darrell. More control for free! image synthesis with semantic diffusion guidance. *arXiv preprint arXiv:2112.05744*, 2021. [3](#)
- [53] Cheng Lu, Yuhao Zhou, Fan Bao, Jianfei Chen, Chongxuan Li, and Jun Zhu. Dpm-solver: A fast ode solver for diffusion probabilistic model sampling in around 10 steps. *arXiv preprint arXiv:2206.00927*, 2022. [2](#)
- [54] Andreas Lugmayr, Martin Danelljan, Andres Romero, Fisher Yu, Radu Timofte, and Luc Van Gool. Repaint: Inpainting using denoising diffusion probabilistic models. In *Proceedings of the IEEE/CVF Conference on Computer Vision and Pattern Recognition*, pages 11461–11471, 2022. [2](#)
- [55] Chenlin Meng, Yang Song, Jiaming Song, Jiajun Wu, Jun-Yan Zhu, and Stefano Ermon. Sdedit: Image synthesis and editing with stochastic differential equations. *arXiv preprint arXiv:2108.01073*, 2021. [2](#), [3](#), [6](#), [16](#)

- [56] Ron Mokady, Amir Hertz, Kfir Aberman, Yael Pritch, and Daniel Cohen-Or. Null-text inversion for editing real images using guided diffusion models. *arXiv preprint arXiv:2211.09794*, 2022. 16
- [57] Alex Nichol, Prafulla Dhariwal, Aditya Ramesh, Pranav Shyam, Pamela Mishkin, Bob McGrew, Ilya Sutskever, and Mark Chen. Glide: Towards photorealistic image generation and editing with text-guided diffusion models. *arXiv preprint arXiv:2112.10741*, 2021. 2, 3
- [58] Alexander Quinn Nichol and Prafulla Dhariwal. Improved denoising diffusion probabilistic models. In *International Conference on Machine Learning*, pages 8162–8171. PMLR, 2021. 3, 6
- [59] Taesung Park, Ming-Yu Liu, Ting-Chun Wang, and Jun-Yan Zhu. Semantic image synthesis with spatially-adaptive normalization. In *Proceedings of the IEEE/CVF conference on computer vision and pattern recognition*, pages 2337–2346, 2019. 16
- [60] Taesung Park, Jun-Yan Zhu, Oliver Wang, Jingwan Lu, Eli Shechtman, Alexei Efros, and Richard Zhang. Swapping autoencoder for deep image manipulation. *Advances in Neural Information Processing Systems*, 33:7198–7211, 2020. 8, 13
- [61] Yong-Hyun Park, Mingi Kwon, Junghyo Jo, and Youngjung Uh. Unsupervised discovery of semantic latent directions in diffusion models. *arXiv preprint arXiv:2302.12469*, 2023. 16
- [62] Gaurav Parmar, Krishna Kumar Singh, Richard Zhang, Yijun Li, Jingwan Lu, and Jun-Yan Zhu. Zero-shot image-to-image translation. *arXiv preprint arXiv:2302.03027*, 2023. 16
- [63] Or Patashnik, Zongze Wu, Eli Shechtman, Daniel Cohen-Or, and Dani Lischinski. Styleclip: Text-driven manipulation of stylegan imagery. In *Proceedings of the IEEE/CVF International Conference on Computer Vision*, pages 2085–2094, 2021. 3
- [64] Aditya Ramesh, Prafulla Dhariwal, Alex Nichol, Casey Chu, and Mark Chen. Hierarchical text-conditional image generation with clip latents. *arXiv preprint arXiv:2204.06125*, 2022. 2
- [65] Robin Rombach, Andreas Blattmann, Dominik Lorenz, Patrick Esser, and Björn Ommer. High-resolution image synthesis with latent diffusion models. In *Proceedings of the IEEE/CVF Conference on Computer Vision and Pattern Recognition*, pages 10684–10695, 2022. 2
- [66] Chitwan Saharia, William Chan, Saurabh Saxena, Lala Li, Jay Whang, Emily Denton, Seyed Kamyar Seyed Ghasemipour, Burcu Karagol Ayan, S Sara Mahdavi, Rapha Gontijo Lopes, et al. Photorealistic text-to-image diffusion models with deep language understanding. *arXiv preprint arXiv:2205.11487*, 2022. 2
- [67] Vikash Sehwal, Caner Hazirbas, Albert Gordo, Firat Ozgenel, and Cristian Canton. Generating high fidelity data from low-density regions using diffusion models. In *Proceedings of the IEEE/CVF Conference on Computer Vision and Pattern Recognition*, pages 11492–11501, 2022. 3
- [68] Yujun Shen, Ceyuan Yang, Xiaoou Tang, and Bolei Zhou. Interfacegan: Interpreting the disentangled face representation learned by gans. *IEEE transactions on pattern analysis and machine intelligence*, 2020. 3
- [69] Jiaming Song, Chenlin Meng, and Stefano Ermon. Denoising diffusion implicit models. *arXiv preprint arXiv:2010.02502*, 2020. 2, 3
- [70] Yang Song, Jascha Sohl-Dickstein, Diederik P Kingma, Abhishek Kumar, Stefano Ermon, and Ben Poole. Score-based generative modeling through stochastic differential equations. *arXiv preprint arXiv:2011.13456*, 2020. 2, 3, 6, 16
- [71] Narek Tumanyan, Michal Geyer, Shai Bagon, and Tali Dekel. Plug-and-play diffusion features for text-driven image-to-image translation. *arXiv preprint arXiv:2211.12572*, 2022. 16
- [72] Bram Wallace, Akash Gokul, and Nikhil Naik. Edict: Exact diffusion inversion via coupled transformations. *arXiv preprint arXiv:2211.12446*, 2022. 16
- [73] Ting-Chun Wang, Ming-Yu Liu, Jun-Yan Zhu, Andrew Tao, Jan Kautz, and Bryan Catanzaro. High-resolution image synthesis and semantic manipulation with conditional gans. In *Proceedings of the IEEE conference on computer vision and pattern recognition*, pages 8798–8807, 2018. 16
- [74] Daniel Watson, William Chan, Jonathan Ho, and Mohammad Norouzi. Learning fast samplers for diffusion models by differentiating through sample quality. In *International Conference on Learning Representations*, 2022. 3
- [75] Zijie Wu, Zhen Zhu, Junping Du, and Xiang Bai. Ccpl: Contrastive coherence preserving loss for versatile style transfer. In *European Conference on Computer Vision*, pages 189–206. Springer, 2022. 8, 13
- [76] Shaoan Xie, Zhifei Zhang, Zhe Lin, Tobias Hinz, and Kun Zhang. Smartbrush: Text and shape guided object inpainting with diffusion model. *arXiv preprint arXiv:2212.05034*, 2022. 16
- [77] Keiji Yanai and Ryosuke Tanno. Conditional fast style transfer network. In *Proceedings of the 2017 ACM on International Conference on Multimedia Retrieval*, pages 434–437, 2017. 3
- [78] Binxin Yang, Shuyang Gu, Bo Zhang, Ting Zhang, Xuejin Chen, Xiaoyan Sun, Dong Chen, and Fang Wen. Paint by example: Exemplar-based image editing with diffusion models. *arXiv preprint arXiv:2211.13227*, 2022. 16
- [79] Jaejun Yoo, Youngjung Uh, Sanghyuk Chun, Byeongkyu Kang, and Jung-Woo Ha. Photorealistic style transfer via wavelet transforms. In *Proceedings of the IEEE/CVF International Conference on Computer Vision*, pages 9036–9045, 2019. 16
- [80] Fisher Yu, Ari Seff, Yinda Zhang, Shuran Song, Thomas Funkhouser, and Jianxiong Xiao. Lsun: Construction of a large-scale image dataset using deep learning with humans in the loop. *arXiv preprint arXiv:1506.03365*, 2015. 6
- [81] Oğuz Kaan Yüksel, Enis Simsar, Ezgi Gülperi Er, and Pinar Yanardag. Latentclr: A contrastive learning approach for unsupervised discovery of interpretable directions. In *Proceedings of the IEEE/CVF International Conference on Computer Vision*, pages 14263–14272, 2021. 3
- [82] Lvmin Zhang and Maneesh Agrawala. Adding conditional control to text-to-image diffusion models. *arXiv preprint arXiv:2302.05543*, 2023. 16

- [83] Ye Zhu, Yu Wu, Zhiwei Deng, Olga Russakovsky, and Yan Yan. Boundary guided mixing trajectory for semantic control with diffusion models. *arXiv preprint arXiv:2302.08357*, 2023. [6](#), [16](#)

# Training-free Style Transfer Emerges from h-space in Diffusion models

## Supplementary Material

### Table of Contents

A. Implementation details	13
B. Varying the strength of content injection	13
C. Effect of style calibration	13
D. More results and comparison	13
E. More analyses of Slerp	14
F. Discussion details	16
G. $\gamma$ scheduling	16
H. More related work	16
I. Stable diffusion experiment details	16

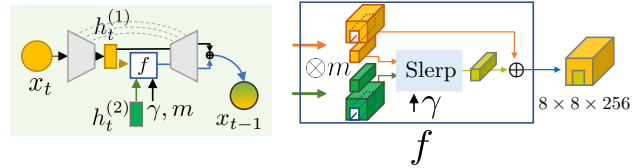


Figure S1: **Illustration of spatial content injection methods** Mask  $m$  determines the area of feature map. Slerp of masked  $h_t$  enables content injection into designated space.

component along the reverse process, according to Eq. (13), we expect linear change of content in the image by linearly controlling  $\alpha$  that specifies  $\gamma = \alpha^{1/T}$ . Note that we did not consider the influence of the networks for the approximation.

### C. Effect of style calibration

In this section, we present an analysis of the parameter  $\omega$  which controls the strength of the style element. Figure S3 displays the resulting images with sweeping  $\omega$ . As  $\omega$  increases, the style elements become more prominent. When  $\omega$  equals 0, the result is without style calibration. We note that style calibration with  $\omega = 0$  is not rigorously defined. In Figure S4, we observe a trade-off between Gram loss and ID similarity, as well as FID, depending on the value of  $\omega$ . However, despite this trade-off, increasing  $\omega$  results in more effective style transfer.

### D. More results and comparison

#### D.1. More qualitative results

We provide more qualitative results of CelebA-HQ, AFHQ, METFACES, LSUN-church, and LSUN-bedroom in Figure S15-S21 (located at the end for compact arrangement).

### A. Implementation details

To perform the reverse process for figures, we used 1000 steps, while for tables and plots, we used 50 steps. During inference, we injected  $h_t$  sparsely only at the timesteps where the content injection was applied within the 50 inference steps. For the remaining timesteps, we used the original DDIM sampling. This approach enabled us to achieve the same amount of content injection across different inference steps.

For local style mixing, we spatially applied Slerp on  $h_t$ , which has a dimension of  $8 \times 8 \times 256$ , as demonstrated in Figure S1. In face swapping, we used a portion of  $h_t$  that corresponds to the face area for Slerp. In § 3, we used the editing interval  $[T=1000, t_{edit}=400]$ , and did not use quality boosting to eliminate stochasticity for comparison purposes, i.e.,  $t_{boost} = 0$ .

### B. Varying the strength of content injection

Figure S2 illustrates the results of content injection with different values of  $\gamma$ . As observed in Figure 7 (b), there is a positive correlation between  $\gamma$  and amount of content change. However, increasing  $\gamma > 0.6$  barely leads to any content change but instead, it degrades the quality of images with distortions and artifacts. As the recursive injection of content by  $\gamma$  exponentially decreases the original  $h_t$

	Method	Preference (%)
Content injection	Swapping Autoencoder [60]	40.11
	Ours	<b>59.89</b>
Local content injection	StyleMapGAN [44]	33.56
	Ours	<b>66.44</b>
Artistic style transfer	StyTr <sup>2</sup> [19]	20.89
	CCPL [75]	21.44
	Ours	<b>57.67</b>

Table S1: User study with 90 participants.

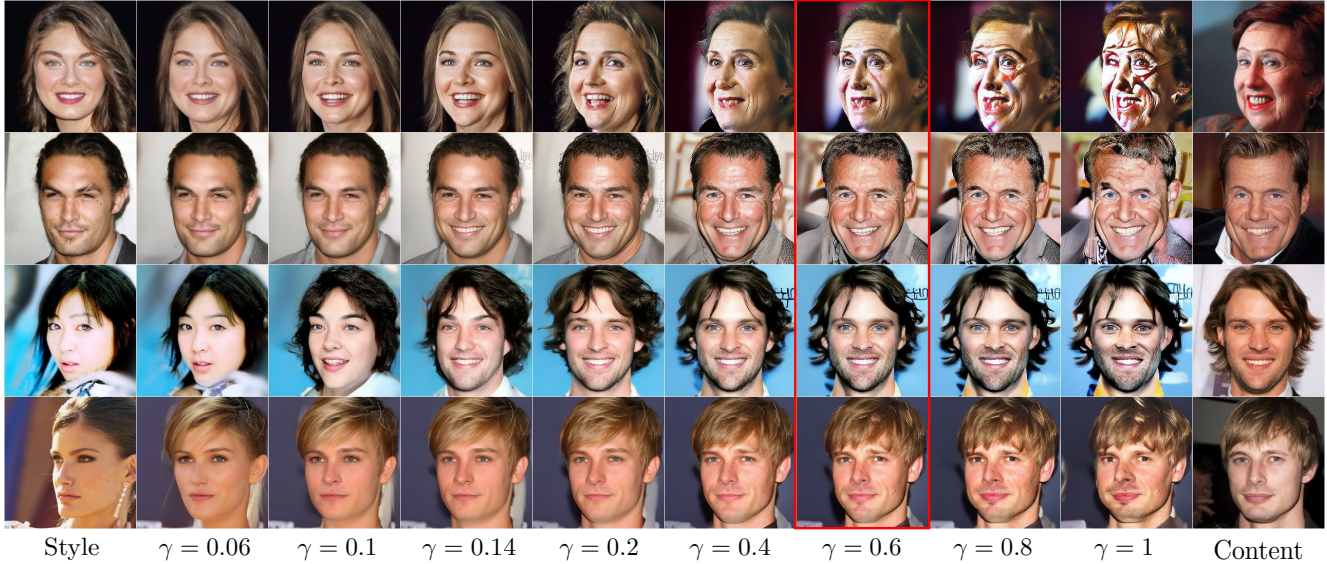


Figure S2:  $\gamma$  controls how much content will be injected. We do not use other techniques such as quality boosting for comparison.

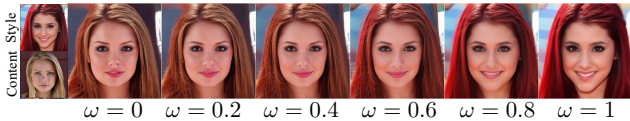


Figure S3: **Effect of increasing  $\omega$ .** Increasing  $\omega$  reflects style elements stronger and  $\omega = 0$  shows the result without style calibration.

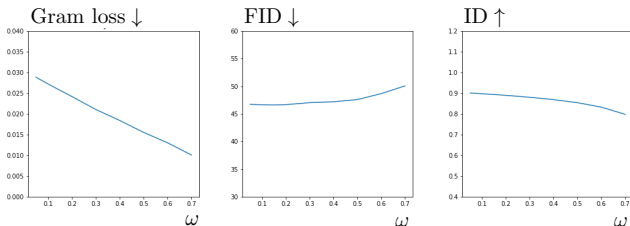


Figure S4: **Quantitative results of style calibration with varying  $\omega$ .** style calibration facilitates style transfer while minimizing content injection loss and maintaining the quality of the resulting images.

## D.2. Comparison with the other methods.

Table S1 presents the results of a user study conducted with 90 participants to compare our method with existing methods. The participants were asked a question: “Which image is more natural while faithfully reflecting the style and the content?”. We randomly selected ten images for content injections and thirty images for style transfer without any curation. The example images are shown in Figure S11-S13 (located at the end for clear spacing).

Even though DiffStyle works on pretrained diffusion models without further training for the task, our method outperformed the others. We selected the recent methods from the respective tasks for comparison.

## D.3. Comparison with a concurrent work

We also provide more qualitative comparison with DiffuseIT [47] in Figure S14. DiffStyle shows comparable results without extra supervision using DINO ViT [7] used by DiffuseIT. As shown in the figure, DiffStyle is highly proficient at accurately and authentically reflecting the style color while avoiding artificial contrast, especially when there is a significant difference in color between the content and the style (e.g., black and white). In contrast, DiffuseIT may not be able to fully capture the style color in these scenarios. This discrepancy is due to the starting point of the reverse process. DiffuseIT utilizes the inverted  $x_T$  of the content image to sample and manipulates noise to match the target style element. The large gap in color distribution between the content and style images makes it challenging for DiffuseIT to overcome this difference entirely. Conversely, DiffStyle initially samples from the inverted  $x_T$  of the style image, making it easier to maintain the color of the style image. The style elements which start from  $x_T$  pass through the skip connection.

## E. More analyses of Slerp

### E.1. Comparison with Lerp

The intuition behind using Slerp is that we should preserve the correlation between  $h_t$  and its matching skip con-

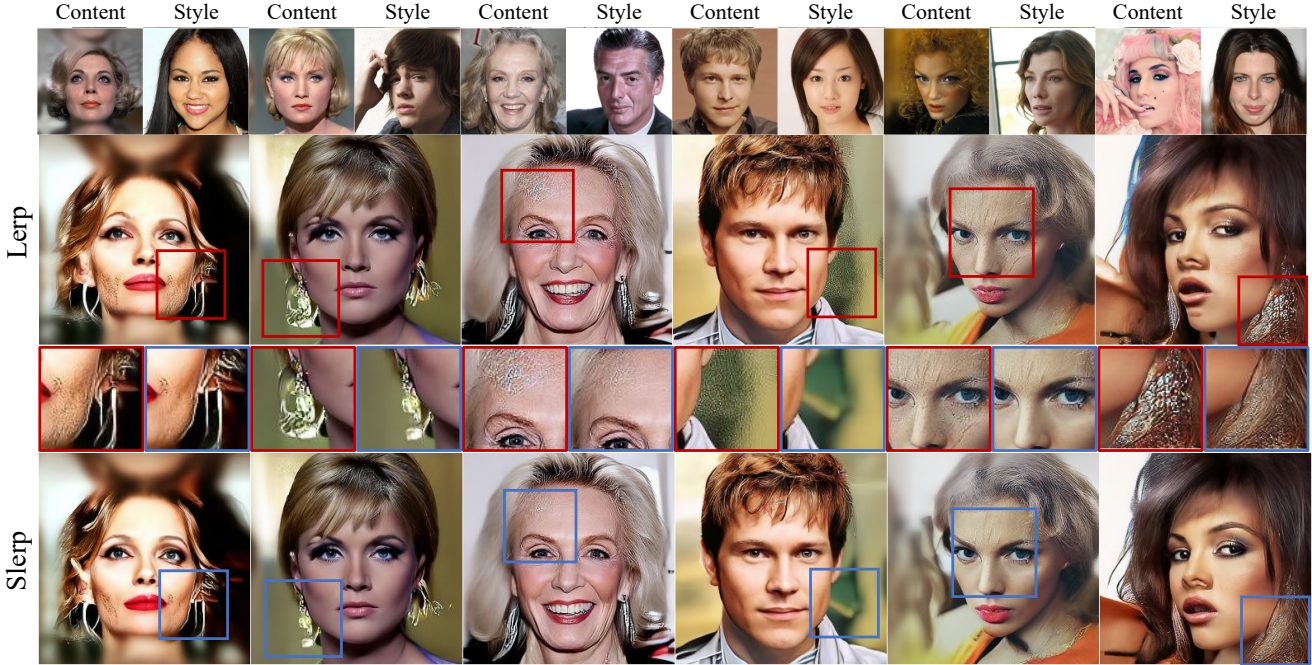


Figure S5: **Comparison between Slerp and Lerp.** Slerp reduces artifacts and distortions in Lerp. Note that We do not use other techniques such as quality boosting to evaluate the effect of Slerp only.

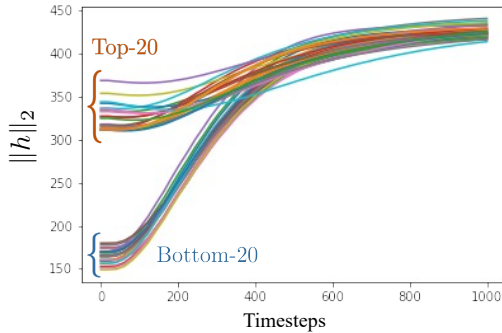


Figure S6: We choose  $h_t$  from top 20 and bottom 20 samples in their norms among 500 samples. Each line represents a trajectory of  $\|h\|_2$  during the reconstruction of a sample.

nection (§ 3.2). Here, we explore an alternative: Lerp. When  $h_t$  and  $h_t^{content}$  have different norms, using Lerp results in more artifacts in the final image as shown in Figure S5. This difference in norms of  $h_t$  is reported in Figure S6. Figure S7 illustrates the difference between Slerp, Lerp, and Lerp followed by normalization. Lerp may change the norm of  $\mathbf{f}(h_t, h_t^{content}, \gamma)$  when the norm of  $h_t$  and  $h_t^{content}$  are different, leading to a decrease in image quality. However, Lerp followed by normalization produces results similar to Slerp. Still, we choose Slerp because it is easier to implement and less prone to errors.

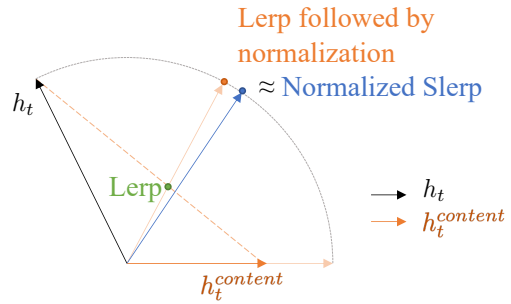


Figure S7: Visual comparison of Slerp and Lerp. The larger difference in norms of  $h_t$  and  $h_t^{content}$  leads to a larger gap between the results. Lerp followed by normalization is closer to Slerp than Lerp.

## E.2. Cumulative content injection

In addition to improving the quality of images, our approach allows us to control the amount of content injection by adjusting the  $h_t$ -to- $h_t^{content}$  ratio through Slerp parameter  $\gamma_t$ . A small  $\gamma_t$  results in a smaller amount of content injection. As mentioned in § 3.1, preserving the  $h_t$  component improves quality. However, there is a trade-off between the content injection rate and quality, and therefore, the value of  $h_t$  needs to be constrained. Further experiments to determine the proper range of  $\gamma$  are discussed in § 4.1.

Note that the effects of Slerp are cumulative along the reverse process as the content injection at  $t$  affects the fol-



Figure S8: **Content image from unseen domain** Other than style images,  $h_t^{content}$  obtained from unseen domain results in poor images.

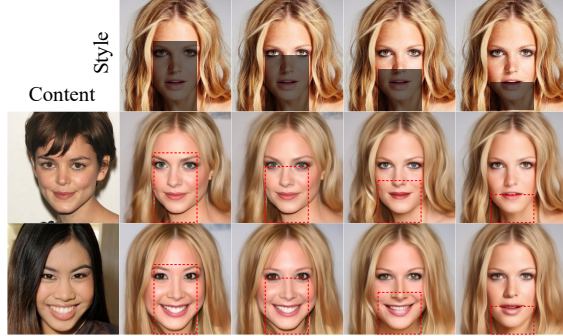


Figure S9: **Local style mixing with various feature map mask sizes.** Adjusting the size and position of feature map mask enables to handle the area of content injection, facilitating control of local style mixing.

lowing reverse process in  $[t - 1, t_{edit}]$ . We provide an approximation of the total amount of injected content as follows. Assuming that the angle between  $h_t$  and  $h_t^{content}$  is close to 0 and the results of content injection at  $t$  are directly passed to the next  $h$ -space at  $t - 1$  without any loss, then

$$\tilde{h}_t = (1 - \gamma)h_t + \gamma h_t^{content} \approx f(h_t, h_t^{content}, \gamma)$$

and

$$h_{t-1} \approx \tilde{h}_t.$$

Along the reverse process,  $\tilde{h}_t$  is recursively fed into the next stage. After  $n$  content injections, we get

$$\tilde{h}_{t-n} \approx (1 - \gamma)^n h_t + \gamma \sum_{i=1}^n (1 - \gamma)^{i-1} h_{t-i}^{content}. \quad (13)$$

As  $0 \leq \gamma \leq 1$ , the proportion of  $h_t$  decreases exponentially and the proportion of  $h_t^{content}$  accumulates during the content injection stage. It indicates that a large proportion of content is injected compared to  $\gamma$  of Slerp. For further details regarding the ablation study on  $\gamma$ , please refer to § 4.1.

## F. Discussion details

As mentioned in § 5, Figure S8 shows that using out-of-domain images as content leads to completely distorted

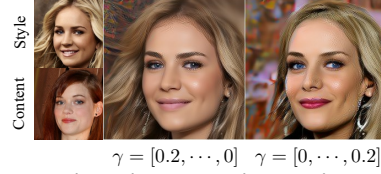


Figure S10: **Various interpolation ratio schedule.**  $\gamma$  is content injection rate.

results. It implies that  $h_t$  cannot be considered a universal representation for all types of content.

Figure S9 shows the local style mixing with various feature map mask sizes. By using the feature map mask, we can designate the specific area where content injection is applied. Unfortunately, the  $h$ -space has small spatial dimensions, limiting the resolution of the mask for local style mixing.

## G. $\gamma$ scheduling

Figure S10 provides the results from alternative schedules. Gradually decreasing the injection along the generative process enhances realism, however, it may not accurately represent the content. Conversely, gradually increasing the injection better preserves the content but results in more artifacts. We kept the total amount of injection fixed in this experiment.

## H. More related work

After [30, 70] proposed a universal approach for Diffusion models (DMs), subsequent works have focused on controlling the generative process of DMs [82, 62, 48, 16, 23, 78, 45, 76, 10, 55, 3, 56, 43, 72]. Especially, [61, 46, 83, 71, 6] have uncovered the role of intermediate feature maps of diffusion models and utilized it for image editing, segmentation, and translation. However, we are the first to analyze the role of the latent variables  $x_t$  in DMs and apply it to style transfer.

The research on controlling the generative process has been done in other generative models such as GANs [27]. [25, 34] introduce style transfer and image-to-image translation with GANs and there have been a number of works that focused on the style of images [31, 13, 12, 79, 4, 59, 73]. After StyleGAN [40, 37, 41], more diverse methodologies have been proposed [44, 41, 12, 44, 14]. However, most of them require training.

## I. Stable diffusion experiment details

We provide more details of experiments with Stable diffusion. In Figure 13, we use conditional random sampling with Stable diffusion v2. In order to apply DiffStyle on Stable diffusion, there are 3 options with conditional guidance. 1) content injection only with unconditional output,



2) content injection only with conditional output, 3) content injection with both conditional/unconditional outputs. We noticed that using only the unconditional output for content injection resulted in poor outcomes, while the other two options produced similar results. Thus, we used only the conditional output for content injection in Figure 13.

Moving on to the implementation details for Stable diffusion, we set the scale to 9.0, used 50 steps for DDIM sampling, and employed the following prompts: for style image, “a highly detailed epic cinematic concept art CG render digital painting artwork: dieselpunk steaming robot” and for content image: “digital painting artwork: a cube-shaped robot with big wheels”, for style image: “8k, wallpaper car” and for content image: “concept, 8k, wallpaper sports car, ferrari bg”, for style image: “a realistic photo of a woman.” and for content image, “a realistic photo of a muscle man.”, style image: “A digital illustration of a small town, 4k, detailed, animation, fantasy” and content image: “A digital illustration of a dense forest, trending in artstation, 4k, fantasy.”



Figure S11: **Qualitative comparison of content injection on FFHQ.** DiffStyle is shown to be effective in reflecting content elements while preserving overall style elements.



Figure S12: **Qualitative comparison of local style mixing on CelebA-HQ.** Despite providing StyleMapGan with detailed segmentation guidance, there are noticeable artifacts in the resulting images, especially at the border lines of the mask. Furthermore, due to the differences in pose between the content and style images, StyleMapGan struggles to seamlessly integrate the two images, resulting in less than optimal outcomes.

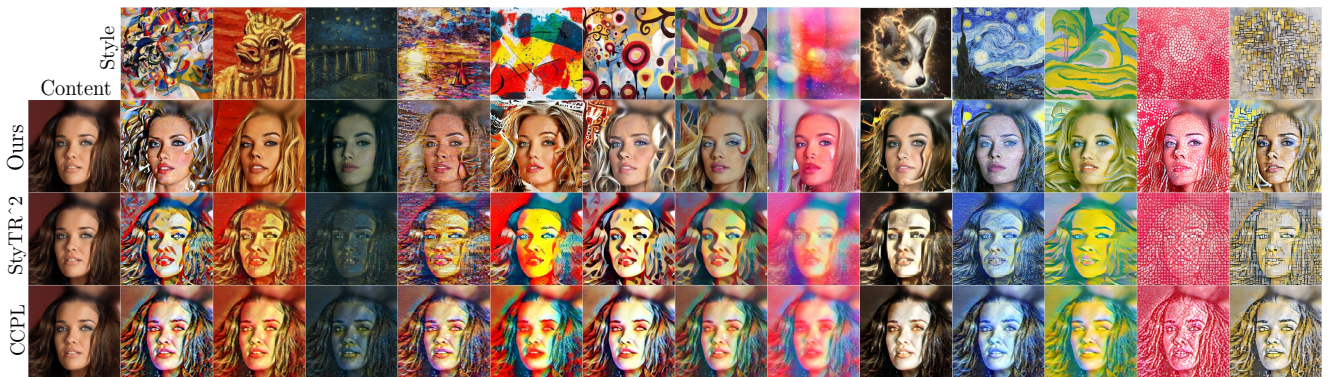


Figure S13: **Qualitative comparison of style transfer with artistic references on CelebA-HQ.** DiffStyle allows using images from unseen domain as style images, enabling style transfer with artistic references. DiffStyle produces harmonization-like effect without severe content distortion. Some styles are better reflected by DiffStyle than the others.



(a) Comparison with DiffuseIT on AFHQ dataset



(b) Comparison with DiffuseIT on CelebA-HQ dataset

Figure S14: **More qualitative comparison with DiffuseIT.** DiffStyle excels in fully and naturally reflecting the style color without creating artificial contrast, particularly when there is a significant gap between the content color and the style color (e.g., black and white). In contrast, DiffuseIT may not fully capture the style color in such cases.



Figure S15: Qualitative results of content injection on CelebA-HQ.

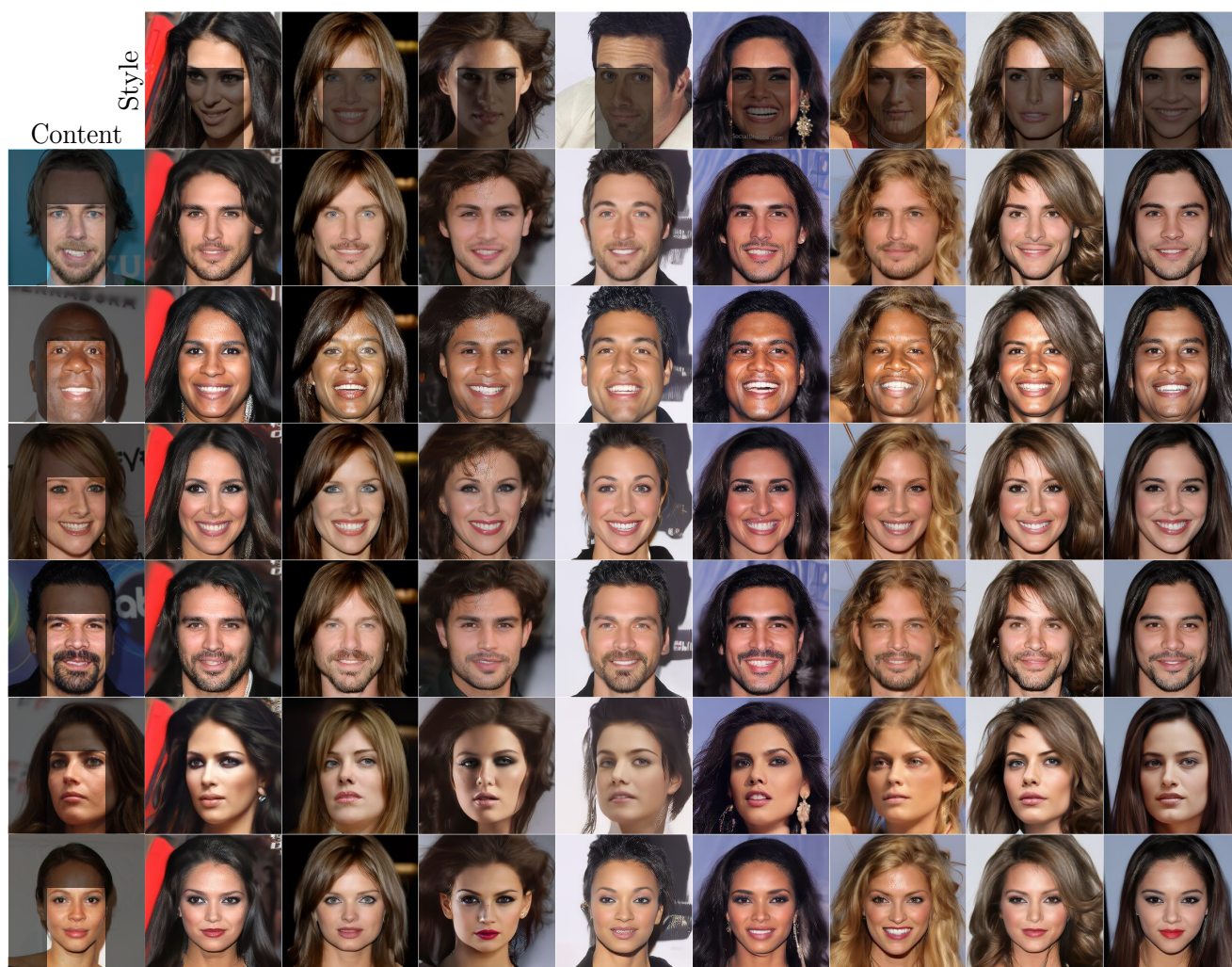


Figure S16: Qualitative results of local editing on CelebA-HQ.



Figure S17: Qualitative results of content injection on AFHQ.



Figure S18: Qualitative results of content injection on METFACES.







Figure S20: Qualitative results of content injection on LSUN-bedroom.

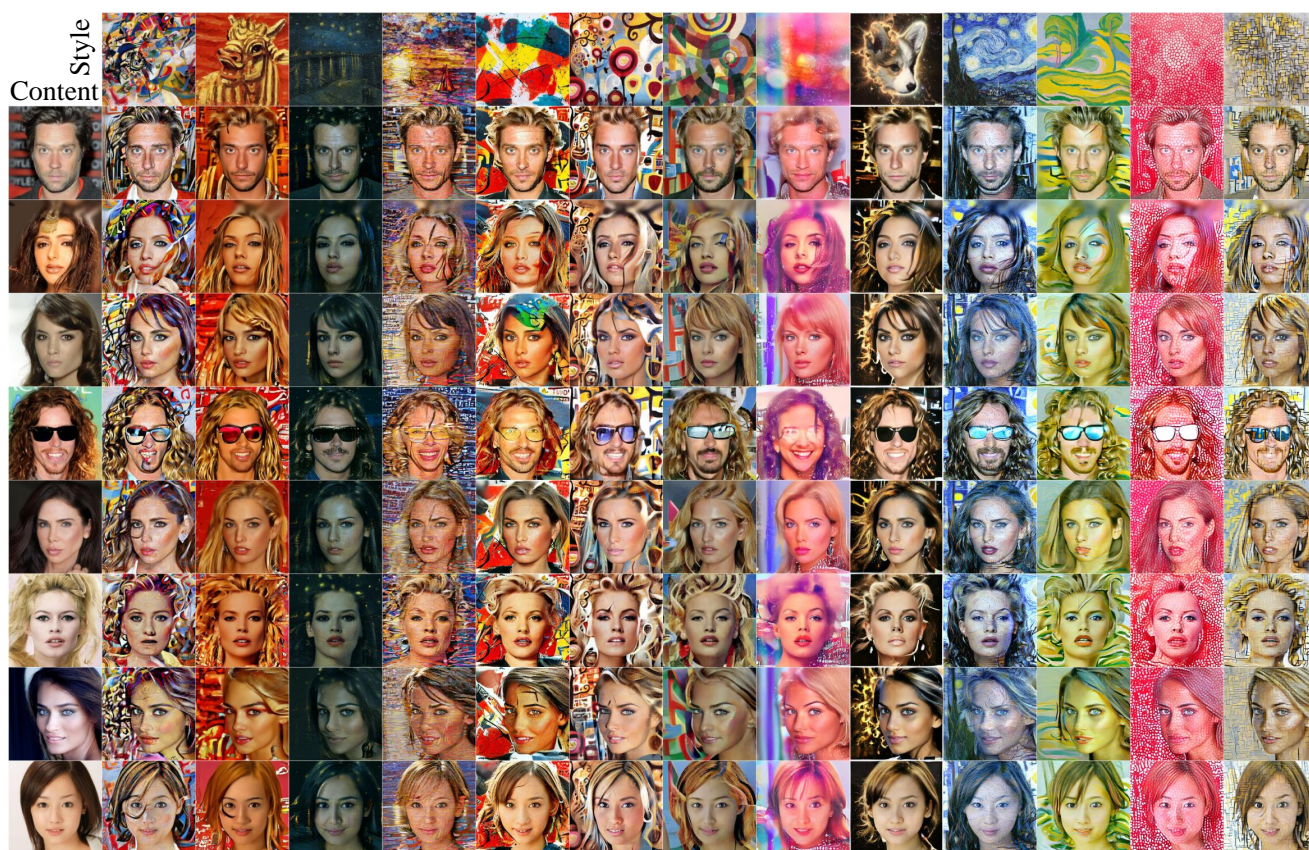


Figure S21: Qualitative results of style transfer with artistic references on CelebA-HQ.